Detection of the Presence of Tornadoes at the Center of Mesocyclones Using Simulated Doppler Velocity Measurements

RODGER A. BROWN AND VINCENT T. WOOD

NOAA/National Severe Storms Laboratory, Norman, Oklahoma

(Manuscript received 21 January 2015, in final form 6 May 2015)

ABSTRACT

Simulations were conducted to investigate the detection of the Doppler velocity tornado signature (TS) and tornadic vortex signature (TVS) when a tornado is located at the center of the parent mesocyclone. Whether the signature is a TS or TVS depends on whether the tornado's core diameter is greater than or less than the radar's effective beamwidth, respectively. The investigation included three radar effective beamwidths, two mesocyclones, and six different-sized tornadoes, each of which had 10 different maximum tangential velocities assigned to it to represent a variety of strengths. The concentric tornadoes and mesocyclones were positioned 10–150 km from the radar. The results indicate that 1) azimuthal shear at the center of the mesocyclone increases as the associated tornado gains strength before a TS or TVS appears, 2) smaller tornadoes need to be much stronger than larger tornadoes at a given range for a signature to appear within the mesocyclone, and 3) when the tornado diameter is wider than about one-quarter of the mesocyclone diameter, the TS or TVS associated with a given mesocyclone appears when the tornado has attained about the same strength regardless of range.

1. Introduction

The majority of strong tornadoes [rated as category 2 or above on the enhanced Fujita scale (EF2+)] are produced within the mesocyclone region of supercell thunderstorms (e.g., Markowski and Richardson 2010). In these instances, it is not clear whether or not the mesocyclone may be masking the presence of a developing tornado until the tornado is strong enough to become obvious in the Doppler velocity measurements. This is likely the situation at distances from a radar where the radar beam is broader. A few simulation studies have been undertaken that show how radar beamwidth, tornado size, and distance from the radar affect the apparent size and strength of the tornado. For example, Wurman and Alexander (2004) use mobile Doppler-on-Wheels (DOW) measurements within a few kilometers of tornadoes to produce simulated reflectivity and Doppler velocity measurements at a 12-km range for several different radars; those radars with the larger effective beamwidths EBWs[1] produced the greatest amount of degradation/smoothing. Wood et al. (2009) use output from the tornado numerical model of Dowell et al. (2005) to show that WSR-88D superresolution with its narrower EBW produces stronger simulated Doppler velocity and reflectivity measurements in tornadoes than with WSR-88D legacy resolution.

When a tornado is sampled by a Doppler radar, there is a distinction between the Doppler velocity signature of a tornado that is larger than the radar's EBW and one that is smaller. When the tornado's core diameter CD is larger than the EBW, the Doppler velocity signature is called a tornado signature (TS) because it represents some semblance of the tornado's size and strength (e.g., Brown 1998). However, as discovered in the Union City, Oklahoma, tornadic storm on 24 May 1973, a tornadic vortex signature (TVS)—consisting of extreme Doppler velocity values of opposite sign that are separated in the azimuthal direction by approximately one EBW—arises

Corresponding author address: Dr. Rodger A. Brown, NOAA/National Severe Storms Laboratory, 120 David L. Boren Blvd., Norman, OK 73072.
E-mail: rodger.brown@noaa.gov

DOI: 10.1175/WAF-D-15-0014.1

[1] When a radar antenna scans azimuthally while it is collecting a sufficient number of samples to compute representative values of radar variables, the data are smoothed somewhat as if the horizontal width of the radar beam were wider than the transmitted beam. The width of the hypothetically widened beam is called the effective beamwidth (e.g., Doviak and Zrnić 1993, 193–197; Brown et al. 2002).

when the tornado is smaller than the EBW (Brown et al. 1978). Based on simulations, Brown et al. (1978) found that the strength of the TVS is independent of tornado size or strength; so all one can say is that a tornado is present when there is a TVS. Subsequent simulations by Wood and Brown (2011) also find that the extreme Doppler velocity values of the TVS are unaffected by the choice of vortex model or whether the vortex is one celled (updraft only) or two celled (central downdraft surrounded by updraft).

Based on our perusals of Doppler velocity fields within evolving tornadic storms, it appears that shear at the center of the mesocyclone increases before the appearance of a TS or TVS. To investigate the evolving shear and to determine under what conditions a TS or TVS emerges from the background mesocyclone signature, we conducted simulations of tornadoes at the center of mesocyclones using the following variables: EBW, tornado and mesocyclone size and strength, and range from radar. The results of this investigation are discussed in the following sections.

2. Method

Mobile Doppler radar observations near tornadoes and their parent mesocyclones reveal a wide range of variations (e.g., Wurman and Kosiba 2013). However, for this simulation study, we made several simplifying assumptions. We used a single one-celled axisymmetric tornado centered within a one-celled axisymmetric parent mesocyclone—both rotating cyclonically. To represent some of the variety found in nature, we used combinations of six tornado and two mesocyclone sizes, each with different characteristics as listed in Table 1. We further assumed that the vortices were vertical and uniform with height throughout the depth sampled by the quasihorizontal radar beam.

The Burgers–Rott tangential velocity V_x profile (e.g., Davies–Jones 1986), which is a good axisymmetric approximation for tornadoes (e.g., Bluestein et al. 2007; Kosiba and Wurman 2010), was used for both tornadoes and mesocyclones. With the Burgers–Rott profile, tangential velocity increases from zero at the vortex center to a broadly peaked maximum at the core radius and then slowly decreases with increasing radius. Reflectivity across each simulated mesocyclone was a uniform 40 dBZ. To represent centrifuging of hydrometeors and debris by tornadoes, there was a reflectivity minimum at the center of the tornado and a ring of maximum reflectivity at a distance equal to twice the core radius of the tangential velocity profile; the procedure for computing the reflectivity profile is discussed in the appendix. The resulting reflectivity profile associated with each tornado was added to the mesocyclone's uniform reflectivity, producing a reflectivity profile that was uniform only outside the tornado.

TABLE 1. Core diameter and max V_x for the six tornadoes and two mesocyclones used in the simulations. For each tornado, 11 separate simulations of the tornado's peak tangential velocity were conducted by varying the values from 0 m s^{-1} (representing the mesocyclone only) up through 100 m s^{-1} at 10 m s^{-1} intervals.

Vortex	CD (km)	V_x (m s^{-1})
Tornado 1	0.2	0–100 at interval of 10
Tornado 2	0.4	0–100 at interval of 10
Tornado 3	0.6	0–100 at interval of 10
Tornado 4	0.8	0–100 at interval of 10
Tornado 5	1.0	0–100 at interval of 10
Tornado 6	1.2	0–100 at interval of 10
Mesocyclone 1	3.0	40
Mesocyclone 2	5.0	25

Radars having EBWs of 1.0° (approximating WSR-88D superresolution, Terminal Doppler Weather Radar), 1.5° [approximating WSR-88D legacy resolution, Multifunction Phased Array Radar with beam perpendicular to the antenna (e.g., Heinselman et al. 2008)], and 2.0° [approximating the Collaborative Adaptive Sensing of the Atmosphere (CASA) Phased Array Radar with beam perpendicular to the antenna (e.g., Hopf et al. 2009) and the Multifunction Phased Array Radar at ±45° from the perpendicular] were used to scan the vortices. We used the Doppler radar simulator of Wood and Brown (1997), where azimuthal beam shape was Gaussian with full width being 3 times wider than the half-power effective beamwidth (e.g., Doviak and Zrnić 1993, chapter 7). We scanned a single range gate through the center of the vortices; the range gate had a pulse depth of 240 m and it was trapezoidal in shape.

Simulation of the Doppler velocity profile across the tornado and mesocyclone was carried out in the following manner. For each EBW, mesocyclone, and tornado size at a given range, 11 separate simulations of the tornado's peak tangential velocity were conducted by varying the values from 0 m s^{-1} (representing the mesocyclone only) up through 100 m s^{-1} at 10 m s^{-1} intervals. The mesocyclone/tornado center was located at ranges from 10 to 150 km at 10-km intervals from the radar. The mean Doppler velocity within the radar beam (dimensions of full beamwidth by pulse depth) was computed by sampling the reflectivity-weighted tangential velocity curve at hundreds of points across the beam in the azimuthal direction and 11 points in range across the pulse depth. Then, the beam was moved 0.01° in the azimuthal direction and a new mean Doppler velocity value was computed. This process continued

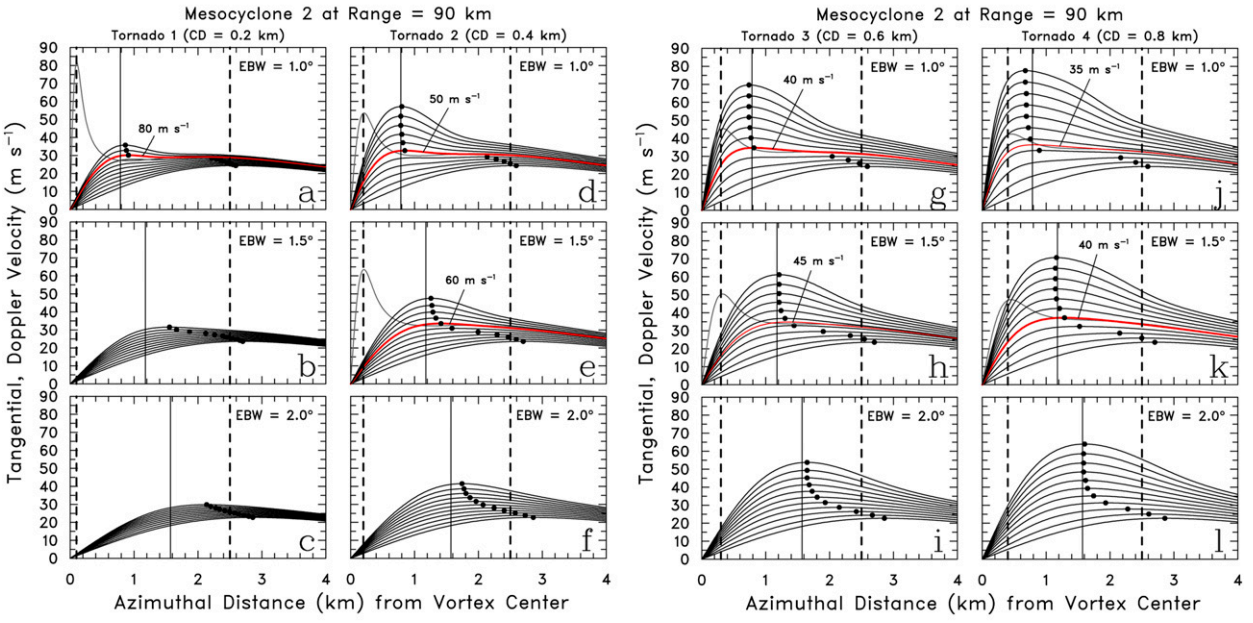

FIG. 1. Simulated Doppler velocity curves on the positive Doppler velocity side of cyclonic tornadoes 1–4 located at the center of mesocyclone 2, 90 km from the radar; the portions of the curves on the negative side (not shown) are negative mirror images of those on the positive side. The 11 curves are Doppler velocity measurements associated with tornadoes having peak tangential velocities of 0–100 m s^{-1} at 10 m s^{-1} intervals, where the lowest curve (0 m s^{-1}) is mesocyclone only. The location of the strongest Doppler velocity value along each curve is indicated by a dot. The red curve indicates the min tornado strength for a TVS to be apparent above the background mesocyclone; it is labeled with the tornado's peak tangential velocity associated with the curve. The gray curve that peaks at the left vertical dashed line is the combined tornado and mesocyclone tangential velocity curve that resulted in the red Doppler velocity curve. The solid vertical line represents the edge of the right half of the effective beamwidth centered on the vortex centers. The beam was so broad relative to the tornado size in (b),(c),(f),(i), and (l) that a TVS was not identified because the peak Doppler velocity value was closer to the mesocyclone core radius (right dashed vertical line) than to the tornado core radius (left dashed vertical line).

until the center of the beam had moved across the mesocyclone core region. Consequently, the result of each simulation was a quasi-continuous mean Doppler velocity curve across the tornado and mesocyclone, as opposed to Doppler velocity values being sampled at discrete azimuthal intervals as measured by an actual radar.

3. Results

As a representative example of what the positive half of the simulated Doppler velocity curves look like, shown in Fig. 1 are those curves produced for tornadoes 1–4 at the center of mesocyclone 2 and sampled at a range of 90 km by radars having EBWs of 1.0°, 1.5°, and 2.0°. Owing to the width of the radar beam at 90-km range, no TSs occur. The determination of which tangential velocity curves indicate the presence of a TVS was based on the assumption that the noticeable peak (dot) in the positive portion of the Doppler velocity curve had to be near the edge of the EBW (vertical solid line) because the positive and negative peaks of a TVS are separated by approximately one EBW or less (e.g., Brown et al. 1978; Brown and Wood 2012); the dots are (nearly) vertically aligned when the TVS is present. When the mesocyclone dominates the Doppler velocity profile, the peaks are closer to the mesocyclone core radius (right dashed line in Fig. 1) than to the tornado core radius (left dashed line in Fig. 1). As the beamwidth of the radar increases, selection of the curves that represent the presence of a TVS becomes more arbitrary because there is no longer a sharp break between dots representing the tornado peak Doppler velocity values and those representing mesocyclone peak values.

Several basic characteristics can be noted in Fig. 1. One characteristic is that Doppler velocity shear—measured when the radar scans in the azimuthal direction across the mesocyclone center—increases significantly in magnitude as the tornado becomes stronger before the TVS becomes apparent. Therefore, if an increase in azimuthal shear becomes evident at the center of a mesocyclone, it is likely that a developing tornado is present that has not yet grown strong enough to produce a TS or TVS. Owing to the increase of the width of the beam with increasing range from the radar, no specific shear threshold value can be established to indicate when a recognizable signature will appear.

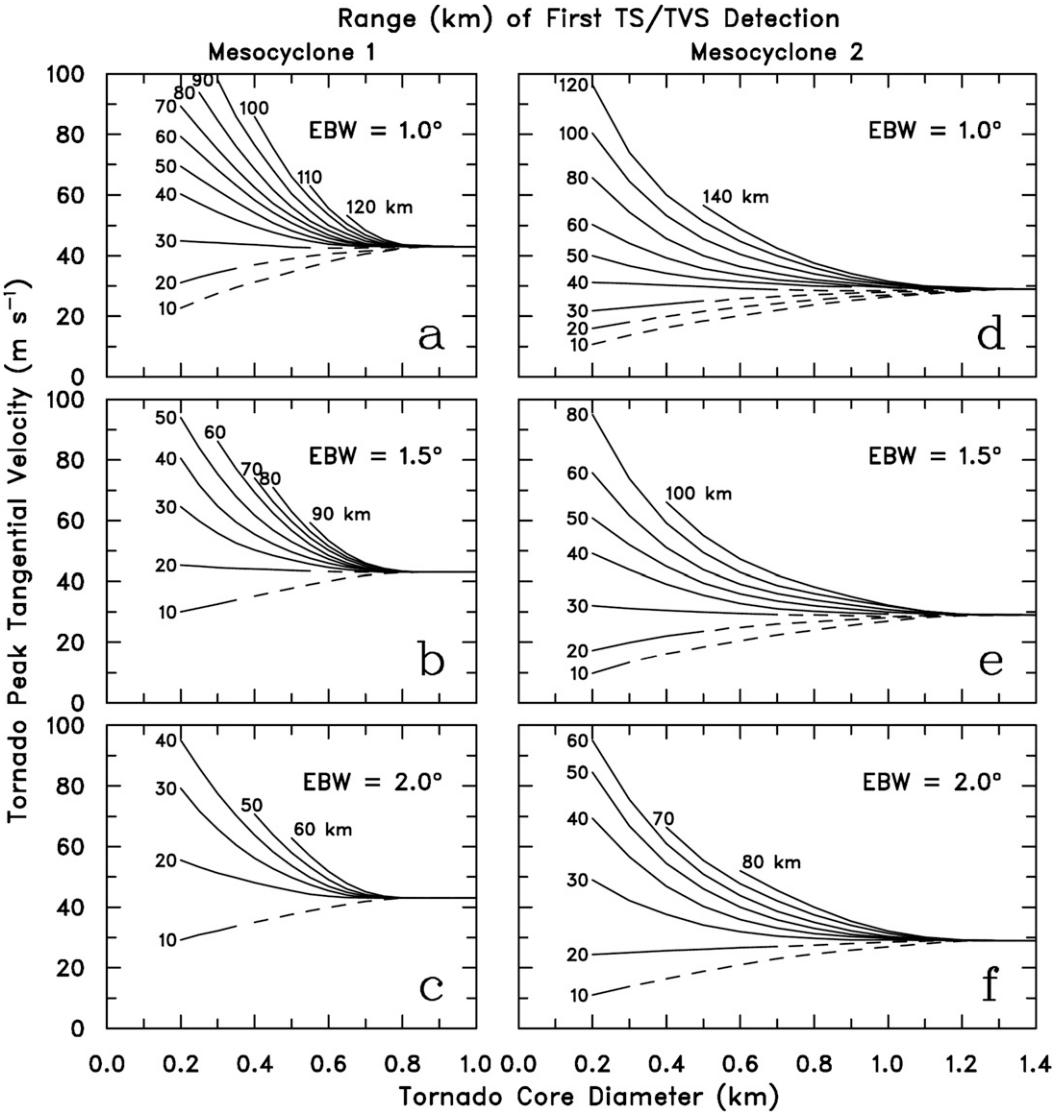

FIG. 2. Smoothed range curves (km) representing the range where the first signature detection occurs as a function of tornado diameter and peak tangential velocity. The portion of the range curve where the first TS (TVS) detection occurs is dashed (solid). (left) Tornadoes located at the center of mesocyclone 1 (CD = 3.0 km, $V_x = 40\ \mathrm{m\ s^{-1}}$) and (right) tornadoes located at the center of mesocyclone 2 (CD = 5.0 km, $V_x = 25\ \mathrm{m\ s^{-1}}$). Curves are given for the three EBWs simulated in this study. The shorter curves at greater ranges end where the peak Doppler velocity value was closer to the mesocyclone core radius than to the tornado core radius (e.g., see tornado 1 in Figs. 1b and 1c).

The influence of beamwidth and tornado size on the appearance of a TVS also is evident in Fig. 1. Some of the results are qualitatively intuitive, but the simulations permit one to attain a quantitative perspective of how various factors influence Doppler velocity signatures. For example, in each column, as beamwidth increases, the strength of the tornado has to increase before a TVS is detected (red curve). As tornado size increases, tangential velocity values within the beam are smoothed to a lesser extent and thus the TVS becomes apparent at a lower Doppler velocity value.

All of the simulated TVS data for the two mesocyclones, six tornadoes, and three EBWs are summarized in Fig. 2. The figure is properly interpreted relative to the range where the first TS or TVS is detected. For example, following a given range curve, as tornado size increases, the tornado's peak tangential velocity does not have to be as strong before a TS or TVS appears. As range of detection increases for a given peak tangential velocity, tornado size has to increase before a TS or TVS appears. As range increases for a given sized tornado, tornado strength must increase.

The peak Doppler velocity value to which curves converge is higher (approximately 43 m s^{-1}) for stronger mesocyclone 1 than the approximately 29 m s^{-1} for weaker mesocyclone 2. Restated, when the mesocyclone is stronger, the tornado has to be stronger before the TS/TVS appears. Also, the tornado core diameter at which curves converge is wider for the larger mesocyclone 2 (core diameter of 5 km) than for mesocyclone 1 (core diameter of 3 km). The ratios of the tornado core diameters to mesocyclone core diameters at the convergence point are approximately the same—being about 0.27 for mesocyclone 1 and about 0.25 for mesocyclone 2.

The range at which a TS/TVS first appears in Figs. 1 and 2 is based on a quasi-continuous azimuthal Doppler velocity curve. In reality, Doppler velocity data are collected at discrete azimuthal intervals, which means that the peak values may be missed. Also, simplifying assumptions were used for the simulations. Consequently, the ranges presented for TVS detections are only approximations of those observed in nature.

4. Concluding comments

When a tornado occurs at the center of the parent mesocyclone in a supercell thunderstorm, its Doppler velocity signature does not become apparent until after the signature becomes stronger than the Doppler velocity signature of the mesocyclone. Whether the tornado's signature is a TS or TVS depends on whether the tornado's core diameter is greater than or less than the radar's EBW, respectively. In this unique study, we have shown how the parent mesocyclone and the radar's EBW can affect the detection of a TS/TVS at various ranges from the radar.

We found that an early indication of potential tornado development is an increase in azimuthal Doppler velocity shear as the radar scans across the mesocyclone center. In fact, each family of curves in Fig. 1 could be interpreted to represent the strengthening of a tornado over time. As the tornado strengthens, the Doppler velocity signature becomes increasingly dominant relative to the mesocyclone signature. The curves in Fig. 2 summarize the ranges at which TSs/TVSs first became obvious for all of the simulations. Though we simulated only two mesocyclones, the results indicate the types of influences that mesocyclones can have on the detection of Doppler velocity signatures of tornadoes.

Acknowledgments. We appreciate comments on an earlier version of this paper made by Pamela Heinselman, Travis Smith, and Arthur Witt. The two anonymous reviewers provided very helpful and insightful comments.

TABLE A1. Values used in Eqs. (A1)–(A3) to compute W_1 and W_2 for tornado 4 as a function of peak tangential velocity where $Z'_{\max} = 25$ dBZ, CR = 400 m, $r_x = 2$CR = 800 m, and $Z^*_{\min} = Z'_{\max} + Z'_{\min}$ at $r = 0$. Since the reflectivity profile across the center of a tornado as a function of peak tangential velocity is not known in reality, the values used for this and the other simulated tornadoes are subjective estimates of what the values might be in a tornado based on various mobile Doppler radar measurements.

V_x	$Z_{r=r_x} - Z_{\text{un}}$	$Z_{r=r_x}$	$Z^*_{\min}$	$Z_{r=0}$	$Z'_{\min}$	W_1	W_2
0	0	40	0	40	−25	1185	1185
10	1	41	−2	38	−27	1380	1270
20	2	42	−7	33	−32	1370	1135
30	3	43	−15	25	−40	1395	1038
40	4	44	−25	15	−50	1443	971
50	5	45	−40	0	−65	1494	909
60	6	46	−55	−15	−80	1559	870
70	7	47	−75	−35	−100	1626	833
80	8	48	−100	−60	−125	1698	800
90	9	49	−125	−85	−150	1777	775
100	10	50	−150	−110	−175	1864	755

APPENDIX

Simulated Reflectivity Profile across a Tornado

In this appendix, we develop an idealized analytical model that simulates a profile through a reflectivity hole and ring of maximum reflectivity around the hole (dBZ) frequently observed with tornadoes sampled by nearby mobile radars (e.g., Wurman and Gill 2000; Bluestein et al. 2007; Wakimoto et al. 2011). The observed reflectivity hole and surrounding ring are functions of the distribution of hydrometeors and debris, tornado strength, and the sensitivity of the radar. For this study, we assume that the reflectivity hole and reflectivity ring are solely a function of tornado strength.

We produce the reflectivity profile by adding together two Gaussian reflectivity profiles: one positive and one negative. The resultant reflectivity profile Z is given by

$$Z(r) = Z'_{\max} \exp\left[-\left(\frac{2r}{W_1}\right)^2\right] + Z'_{\min} \exp\left[-\left(\frac{2r}{W_2}\right)^2\right] + Z_{\text{un}}, \qquad \text{(A1)}$$

where r is the radial distance from the center of the hole, $Z'_{\max}$ ($Z'_{\min}$) is the maximum (minimum) reflectivity value at $r = 0$, W_1 is the width of the positive Gaussian reflectivity ($Z'_{\max} > 0$) profile at $(2r_x/W_1)^2 = 1$, and W_2 is the width of the negative Gaussian reflectivity ($Z'_{\min} < 0$) profile at $(2r_x/W_2)^2 = 1$. Here, r_x represents the radius of

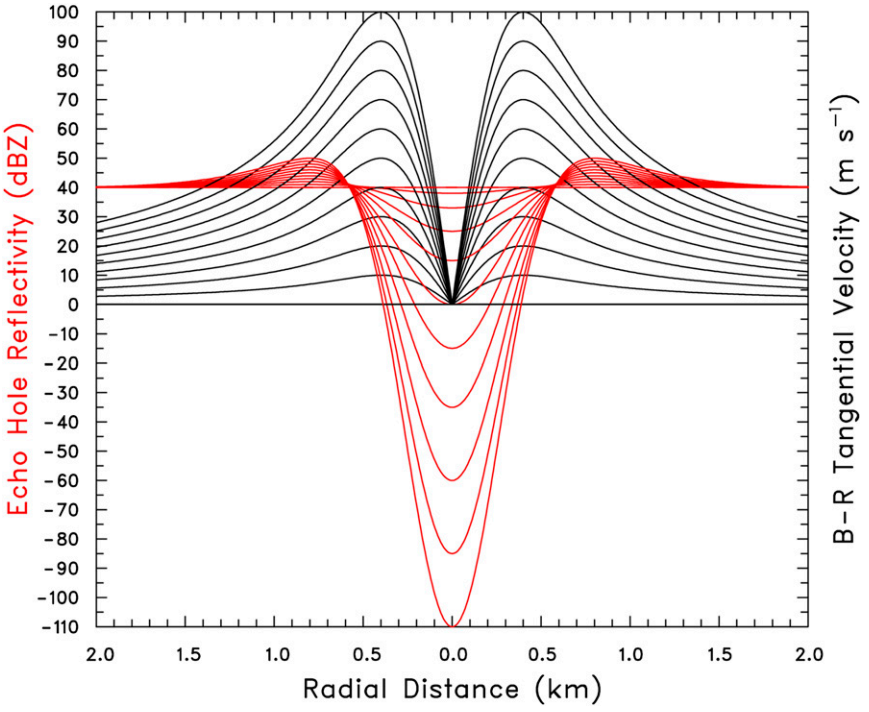

FIG. A1. Profiles of the reflectivity hole and surrounding reflectivity ring (red) across the center of tornado 4 associated with overlaid Burgers–Rott tangential velocity profiles (black). The uniform reflectivity curve at 40 dBZ corresponds to the uniform tangential velocity curve at 0 m s^{-1}. The other reflectivity curves correspond to tangential velocity curves represented by peak values ranging from 10 to 100 m s^{-1} at intervals of 10 m s^{-1}.

the reflectivity ring $Z(r_x)$ (assumed to be twice the core radius CR of the tornado's peak tangential velocity), and $Z_{\rm un}$ (=40 dBZ) is the uniform reflectivity profile across a mesocyclone. The Newton–Raphson method was employed to determine two unknown widths: W_1 and W_2. The equations may be written as

$$f_1(W_1, W_2) = Z'_{\rm max} \exp\left[-\left(\frac{2r_x}{W_1}\right)^2\right] + Z'_{\rm min} \exp\left[-\left(\frac{2r_x}{W_2}\right)^2\right] + Z_{\rm un} - Z(r_x) = 0 \quad \text{(A2)}$$

and

$$f_2(W_1, W_2) = \frac{\partial Z(r_x)}{\partial r_x} = W_1^{-2} Z'_{\rm max} \exp\left[-\left(\frac{2r_x}{W_1}\right)^2\right] + W_2^{-2} Z'_{\rm min} \exp\left[-\left(\frac{2r_x}{W_2}\right)^2\right] = 0. \quad \text{(A3)}$$

The reason for differentiating $Z(r_x)$ with respect to r_x in Eq. (A3) is because a second equation is needed to solve a set of simultaneous nonlinear equations for determining the two unknowns during an iterative process. The Newton–Raphson method requires an initial guess for a starting vector $\mathbf{x}_k = \mathbf{x}_0 = (x_{10}, x_{20})^{\rm T}$ to be estimated for initializing the vector. We chose $x_{10} = 2r_x$ and $x_{20} = 2$CR. These guesses must be near enough to a solution to give convergence in Eqs. (A2) and (A3). When W_1 and W_2 have been determined numerically (an example for tornado 4 is shown in Table A1), the resultant profile across the reflectivity hole and surrounding reflectivity ring (see example in Fig. A1) is obtained using Eq. (A1). It is important to note that $W_1 > W_2 > 0$ in order to produce a localized peak reflectivity value of $Z(r)$ at $r = r_x$. If $W_1 = W_2 > 0$, then $Z(r) = Z_{\rm un}$ results in a flat reflectivity profile.

REFERENCES

Bluestein, H. B., C. C. Weiss, M. M. French, E. M. Holthaus, R. L. Tanamachi, S. Frasier, and A. L. Pazmany, 2007: The structure of tornadoes near Attica, Kansas, on 12 May 2004: High-resolution, mobile, Doppler radar observations. *Mon. Wea. Rev.*, **135,** 475–506, doi:10.1175/MWR3295.1.

Brown, R. A., 1998: Nomogram for aiding the interpretation of tornadic vortex signatures measured by Doppler radar. *Wea. Forecasting,* **13,** 505–512, doi:10.1175/1520-0434(1998)013<0505:NFATIO>2.0.CO;2.

——, and V. T. Wood, 2012: The tornadic vortex signature: An update. *Wea. Forecasting,* **27,** 525–530, doi:10.1175/WAF-D-11-00111.1.

——, L. R. Lemon, and D. W. Burgess, 1978: Tornado detection by pulsed Doppler radar. *Mon. Wea. Rev.,* **106,** 29–38, doi:10.1175/1520-0493(1978)106<0029:TDBPDR>2.0.CO;2.

——, V. T. Wood, and D. Sirmans, 2002: Improved tornado detection using simulated and actual WSR-88D data with enhanced resolution. *J. Atmos. Oceanic Technol.,* **19,** 1759–1771, doi:10.1175/1520-0426(2002)019<1759:ITDUSA>2.0.CO;2.

Davies-Jones, R. P., 1986: Tornado dynamics. *Thunderstorm Morphology and Dynamics,* 2nd ed., E. Kessler, Ed., University of Oklahoma Press, 197–236.

Doviak, R. J., and D. S. Zrnić, 1993: *Doppler Radar and Weather Observations.* 2nd ed. Academic Press, 562 pp.

Dowell, D. C., C. R. Alexander, J. M. Wurman, and L. J. Wicker, 2005: Centrifuging of hydrometeors and debris in tornadoes: Radar reflectivity patterns and wind-measurement errors. *Mon. Wea. Rev.,* **133,** 1501–1524, doi:10.1175/MWR2934.1.

Heinselman, P. L., D. L. Priegnitz, K. L. Manross, T. M. Smith, and R. W. Adams, 2008: Rapid sampling of severe storms by the National Weather Radar Testbed Phased Array Radar. *Wea. Forecasting,* **23,** 808–824, doi:10.1175/2008WAF2007071.1.

Hopf, A. P., J. L. Salazar, R. Medina, V. Venkatesh, E. J. Knapp, S. J. Frasier, and D. J. McLaughlin, 2009: CASA Phased Array Radar System description, simulation and products. *Proc. Int. Geoscience and Remote Sensing Symp.,* Cape Town, South Africa, IEEE, II-968–II-971.

Kosiba, K., and J. Wurman, 2010: The three-dimensional axisymmetric wind field structure of the Spencer, South Dakota, 1998 tornado. *J. Atmos. Sci.,* **67,** 3074–3083, doi:10.1175/2010JAS3416.1.

Markowski, P., and Y. Richardson, 2010: *Mesoscale Meteorology in Midlatitudes.* Advancing Weather and Climate Science Series, Wiley-Blackwell, 407 pp.

Wakimoto, R. M., N. T. Atkins, and J. Wurman, 2011: The LaGrange tornado during VORTEX2. Part I: Photogrammetric analysis of the tornado combined with single-Doppler radar data. *Mon. Wea. Rev.,* **139,** 2233–2258, doi:10.1175/2010MWR3568.1.

Wood, V. T., and R. A. Brown, 1997: Effects of radar sampling on single-Doppler velocity signatures of mesocyclones and tornadoes. *Wea. Forecasting,* **12,** 928–938, doi:10.1175/1520-0434(1997)012<0928:EORSOS>2.0.CO;2.

——, and ——, 2011: Simulated tornadic vortex signatures of tornado-like vortices having one- and two-celled structures. *J. Appl. Meteor. Climatol.,* **50,** 2338–2342, doi:10.1175/JAMC-D-11-0118.1.

——, ——, and D. C. Dowell, 2009: Simulated WSR-88D velocity and reflectivity signatures of numerically modeled tornadoes. *J. Atmos. Oceanic Technol.,* **26,** 876–893, doi:10.1175/2008JTECHA1181.1.

Wurman, J., and S. Gill, 2000: Finescale radar observations of the Dimmitt, Texas (2 June 1995), tornado. *Mon. Wea. Rev.,* **128,** 2135–2164, doi:10.1175/1520-0493(2000)128<2135:FROOTD>2.0.CO;2.

——, and C. Alexander, 2004: Scales of motion in tornadoes: What radars cannot see, what scale circulation is a tornado. Preprints, *22nd Conf. on Severe Local Storms,* Hyannis, MA, Amer. Meteor. Soc., P11.6. [Available online at https://ams.confex.com/ams/pdfpapers/82353.pdf.]

——, and K. Kosiba, 2013: Finescale radar observations of tornado and mesocyclone structures. *Wea. Forecasting,* **28,** 1157–1174, doi:10.1175/WAF-D-12-00127.1.